

PCCP

Physical Chemistry Chemical Physics

Accepted Manuscript

This article can be cited before page numbers have been issued, to do this please use: Y. Kaneko and K. S. Lackner, *Phys. Chem. Chem. Phys.*, 2022, DOI: 10.1039/D2CP02440C.



This is an Accepted Manuscript, which has been through the Royal Society of Chemistry peer review process and has been accepted for publication.

Accepted Manuscripts are published online shortly after acceptance, before technical editing, formatting and proof reading. Using this free service, authors can make their results available to the community, in citable form, before we publish the edited article. We will replace this Accepted Manuscript with the edited and formatted Advance Article as soon as it is available.

You can find more information about Accepted Manuscripts in the [Information for Authors](#).

Please note that technical editing may introduce minor changes to the text and/or graphics, which may alter content. The journal's standard [Terms & Conditions](#) and the [Ethical guidelines](#) still apply. In no event shall the Royal Society of Chemistry be held responsible for any errors or omissions in this Accepted Manuscript or any consequences arising from the use of any information it contains.

Cite this: DOI: 00.0000/xxxxxxxxxx

Kinetic Model for Moisture-Controlled CO₂ Sorption[†]

Yuta Kaneko^a and Klaus S. Lackner^aReceived Date
Accepted Date

DOI: 00.0000/xxxxxxxxxx

The understanding of the sorption/desorption kinetics is essential for practical applications of moisture-controlled CO₂ sorption. We introduce an analytic model of the kinetics of moisture-controlled CO₂ sorption and its interpretation in two limiting cases. In one case, chemical reaction kinetics on pore surfaces dominates, in the other case, diffusive transport through the sorbent defines the kinetics. We show that reaction kinetics, which is dominant in the first case, can be expressed as a linear combination of 1st and 2nd order kinetics in agreement with the static isotherm equation derived and validated in a previous paper. The interior transport kinetics can be described by non-linear diffusion equations. By combining all carbon species into a single equation, we can eliminate – in certain limits – the source terms associated with chemical reactions. In this case, the governing equation is $\frac{\partial \theta}{\partial t} = -\vec{\nabla} \cdot (-D_{\text{eff}} \vec{\nabla} \theta)$. For a sorbent in a form of a flat sheet or a membrane, one can maintain the same functional form of a diffusion equation by introducing a generalized effective diffusivity D_M that combines contributions from both surface chemical reaction kinetics and interior diffusive transport kinetics. Experimental data of transient CO₂ flux in a preconditioned commercial anion exchange membrane fit well to the 1st order model as long as very dry states are avoided, validating the theory. The observed D_M for a preconditioned commercial anion exchange membrane ranges from 6.6×10^{-14} to 7.1×10^{-14} m² s⁻¹ at 35°C. These small values compared to typical ionic diffusivities imply a very slow kinetics, which will be the largest issue that needs to be addressed for practical application. The collected transient CO₂ flux data are used to predict the magnitude of a continuous CO₂ pumping flux in an active membrane that transports CO₂ against a CO₂ concentration gradient. The pumped CO₂ flux is supported by water flux due to a water concentration gradient.

1 Introduction

Since binding energies are weaker for moisture-controlled sorbents than for strong alkali solution such as aqueous sodium hydroxide solutions, the regeneration of moisture-controlled sorbents is likely more cost effective^{1,2}. In comparison to weak base sorbents that also have lower binding energies³ there is an additional benefit on a cost basis because a part of the energy required to drive this system is obtained from the exergy associated with the evaporation of water into ambient air at a relative humidity of less than 100%. Water is far cheaper than most other sources of exergy. For practical designs, we need to understand the kinetics of sorption and desorption processes. Previously, empirical fits have been used to characterize moisture-controlled CO₂ sorption kinetics^{4,5,6}. However, these fits do not consider rate limiting mechanisms. The kinetics could be restricted not only by chemi-

cal reactions or material properties such as diffusion coefficients but also by various experimental conditions⁷ or the geometry of samples. Therefore, we need to distinguish the kinetics of the materials from other effects. Also, simple generic models for the kinetics have been proposed^{8,9}. However, they are not based on the governing equations of moisture-controlled CO₂ sorption. In this paper, we outline an analytic model to describe the kinetics with a bottom-up approach that starts from the governing equations of moisture-controlled CO₂ sorption and take the influence of experimental conditions into consideration. Based on these theoretical models, we have experimentally collected and analyzed transient CO₂ sorption and desorption flux from and into a sorbent corresponding to the change in the external humidity level. For the experimental studies, we applied preconditioning to a commercially available non-brittle anion exchange membrane and confirmed that it works as a moisture-controlled CO₂ sorbent. The membrane is made from sorbent material alone and does not contain any reinforcement. The geometry of a flat sheet makes the analytic approach easier. To minimize the influence

^a School of Sustainable Engineering & the Built Environment, Arizona State University, Tempe, AZ 85287, United States. Tel: 480-727-2499; E-mail: Klaus.Lackner@asu.edu

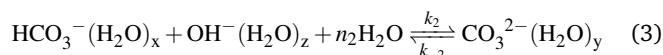
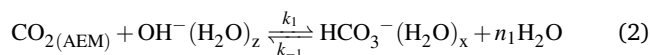
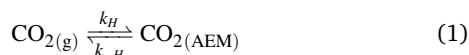
[†] Electronic Supplementary Information (ESI) available. (TBD)

from the experimental conditions, an open-flow experiment has been designed and performed. An open-flow system maintains constant conditions in the gas feed regarding temperature, total pressure, CO₂ concentration and water vapor concentration¹⁰.

2 Kinetic model part I: Chemical reaction kinetics at surfaces of sorbents

In this section, we investigate the case of chemical reactions limiting overall kinetics. This is achieved in case reactions happen at only surfaces and there is no transport to the interior, or fast diffusion transport eliminates chemical gradients in the interior of the materials. Either diffusion does not occur or does not limit the kinetics. For a sufficiently large surface-to-volume ratio (e.g., a very thin membrane), diffusion transport can always be considered fast.

In a previous paper, we identified the following three governing equations for moisture-controlled CO₂ sorption in anionic exchange resins^{11 12 13}:

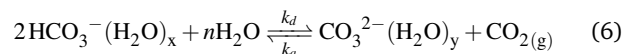


where,

$$n_1 \equiv z - x \quad (4)$$

$$n_2 \equiv y - 1 - x - z \quad (5)$$

Note that ‘‘AEM’’ stands for an anion exchange material. The subscripts g and AEM denote the gaseous and dissolved phase, respectively. They only coexist on the boundaries where Eq.(1) applies. Unlike in the previous paper where we focused on equilibria¹³, in this paper we aim to understand the kinetics of the reaction and consequently flag out the rate constants for forward and backward reactions separately as k_H , k_{-H} , k_1 , k_{-1} , k_2 and k_{-2} . The ratio of the forward and backward reaction rate defines the Henry constant and the equilibrium constants, i.e., $K_{H(\text{AEM})} = k_H/k_{-H}$, $K_{1(\text{AEM})} = k_1/k_{-1}$ and $K_{2(\text{AEM})} = k_2/k_{-2}$. Previously, we noted that the equilibrium concentration of OH⁻ is very small in the regime relevant to CO₂ capture from air¹³. After eliminating OH⁻ terms from these chemical reactions, the overall chemical reaction can be described as^{4 13}



where,

$$n \equiv n_1 + n_2 = y - 2x - 1 \quad (7)$$

The right arrow represents CO₂ desorption with a rate constant k_d , while the left arrow indicates CO₂ absorption with a rate constant k_a . The ratio of sorption and desorption rate defines the equilibrium constant for this combined chemical reaction, i.e., $K_{H(\text{AEM})}K_{1(\text{AEM})}/K_{2(\text{AEM})} = k_a/k_d$. The rate law of the kinetics depends on which reactions are actually elementary reactions¹⁴. Eq.(6) taken as an elementary reaction implies that CO₂ molecules collide with hydrated carbonate ions inside the sorbent for CO₂ absorption and that a hydrated bicarbonate ions to collide with another hydrated bicarbonate ion and n water molecules for desorption. The complexity of this reaction makes it unlikely that Eq.(6) is an elementary reaction. However, we show in section A.2 in the Supplementary Information that the rate law derived assuming that Eq.(1), Eq.(2) and Eq.(3) are elementary reactions can be described as a perturbation of a hypothetical rate law derived from Eq.(6). This hypothetical form of the rate law includes the most important features of the reaction kinetics of moisture-controlled CO₂ sorption even though it omits some of the minor features. Therefore it is instructive to discuss its analytic form. When the concentration of OH⁻ and H⁺ are negligible, the condition of charge neutrality simplifies to

$$[\text{A}] = [\text{HCO}_3^-(\text{H}_2\text{O})_x] + 2[\text{CO}_3^{2-}(\text{H}_2\text{O})_y] \quad (8)$$

where, [A] denotes alkalinity^{13 15}. Generally, [X] represents the concentration of the chemical species X. The concentration of the Dissolved Inorganic Carbon (DIC) in a sorbent is defined as

$$[\text{DIC}] \equiv [\text{CO}_2] + [\text{HCO}_3^-(\text{H}_2\text{O})_x] + [\text{CO}_3^{2-}(\text{H}_2\text{O})_y] \quad (9)$$

We define θ as the carbon loading relative to the alkalinity:

$$\theta \equiv [\text{DIC}]/[\text{A}] \quad (10)$$

$$\sim \{[\text{HCO}_3^-(\text{H}_2\text{O})_x] + [\text{CO}_3^{2-}(\text{H}_2\text{O})_y]\}/[\text{A}] \quad (11)$$

With our additional assumption that [CO₂] is negligible compared to [HCO₃⁻(H₂O)_x] + [CO₃²⁻(H₂O)_y],

$$[\text{HCO}_3^-(\text{H}_2\text{O})_x] = [\text{A}](2\theta - 1) \quad (12)$$

$$[\text{CO}_3^{2-}(\text{H}_2\text{O})_y] = [\text{A}](1 - \theta) \quad (13)$$

Assuming that Eq.(6) is an elementary reaction, sorption rate v_a and desorption rate v_d can be expressed as

$$v_a = k_a P_{\text{CO}_2} [\text{CO}_3^{2-}(\text{H}_2\text{O})_y] \quad (14)$$

$$v_d = k_d [\text{HCO}_3^-(\text{H}_2\text{O})_x]^2 [\text{H}_2\text{O}]^n \quad (15)$$

An overall sorption rate of the DIC on surfaces can be described as

$$\frac{\partial[\text{DIC}]}{\partial t} = \frac{\partial[\text{HCO}_3^-(\text{H}_2\text{O})_x]}{\partial t} + \frac{\partial[\text{CO}_3^{2-}(\text{H}_2\text{O})_y]}{\partial t} \quad (16)$$

$$= [\text{A}] \frac{\partial \theta}{\partial t} \quad (17)$$

$$= v_a - v_d \quad (18)$$

Substituting Eq.(14) and Eq.(15) into Eq.(18) yields

$$\frac{\partial \theta}{\partial t} = \frac{k_d}{[\text{A}]} \left\{ \left(\frac{K_{1(\text{AEM})} K_{H(\text{AEM})}}{K_{2(\text{AEM})}} \right) P_{\text{CO}_2} [\text{CO}_3^{2-}(\text{H}_2\text{O})_y] - [\text{HCO}_3^-(\text{H}_2\text{O})_x] [\text{H}_2\text{O}]^n \right\} \quad (19)$$

$$= \frac{k_d [\text{H}_2\text{O}]^n}{[\text{A}]} \left\{ \left(\frac{K_{1(\text{AEM})} K_{H(\text{AEM})}}{K_{2(\text{AEM})} [\text{H}_2\text{O}]^n} \right) P_{\text{CO}_2} [\text{CO}_3^{2-}(\text{H}_2\text{O})_y] - [\text{HCO}_3^-(\text{H}_2\text{O})_x] \right\} \quad (20)$$

Moving from Eq.(19) to Eq.(20), we rearranged terms to create a rate law with an effective equilibrium constant that depends on water activity. Substituting Eq.(12) and Eq.(13) into Eq.(20) yields

$$\frac{\partial \theta}{\partial t} = [\text{A}] k_d [\text{H}_2\text{O}]^n \left[2K_{\text{eq}(\text{eff})} P_{\text{CO}_2} (1 - \theta) - (\theta - 1)^2 \right] \quad (21)$$

where,

$$K_{\text{eq}(\text{eff})} \equiv K_{\text{eq}} [\text{H}_2\text{O}]^{-n} \quad (22)$$

and

$$K_{\text{eq}} \equiv \frac{k_a/k_d}{2[\text{A}]} = \frac{K_{1(\text{AEM})} K_{H(\text{AEM})}}{2[\text{A}] K_{2(\text{AEM})}} \quad (23)$$

In equilibrium, $\frac{\partial \theta}{\partial t}$ has to be zero, i.e.,

$$4\theta_{\text{eq}}^2 + \theta_{\text{eq}}(2K_{\text{eq}(\text{eff})} P_{\text{CO}_2(\text{eq})} - 4) - 2K_{\text{eq}(\text{eff})} P_{\text{CO}_2(\text{eq})} + 1 = 0 \quad (24)$$

where, the subscript eq denotes the values in equilibrium. This quadratic equation has only one solution in the regime of $0.5 < \theta < 1$:

$$\theta_{\text{eq}} = \frac{P_{\text{CO}_2(\text{eq})} K_{\text{eq}(\text{eff})}}{4} \left\{ \sqrt{1 + \frac{4}{P_{\text{CO}_2(\text{eq})} K_{\text{eq}(\text{eff})}}} - 1 \right\} + \frac{1}{2} \quad (25)$$

The other root of Eq.(24) is in a regime in which the approxi-

mation of negligible OH^- concentrations is not valid and has no physical meaning. This expression for the equilibrium loading (Eq.(25)) is identical to the isotherm equation that has been derived and validated in the previous paper^{13 16}. In the following section, we rewrite Eq.(21) in terms of $\theta - \theta_{\text{eq}}$, which is more useful from an experimental point of view. A common experiment for measuring sorption kinetics changes the environmental condition (e.g. P_{CO_2} or humidity) of the system containing a sorbent from an equilibrated state and measures the temporal profile of the response of the system until a new equilibrated state is achieved. θ_{eq} is θ at a final state in equilibrium with a certain value of a final pressure $P_{\text{CO}_2(\text{eq})}$.

2.1 Sorption kinetics equation for an open system.

In typical open-flow experiments, gas flows over the sample. The experimenter maintains a controlled chemical composition in the feed stream and observes the chemical composition in the out-flow. In particular implementation, one maintains a constant P_{CO_2} in the input until the sample is in equilibrium with that stream. The gas composition downstream of the sample will be different from the input composition until the equilibrium reaches. Combining Eq.(21) and Eq.(24) yields (see section A.1 in the Supplementary Information):

$$\frac{\partial \theta}{\partial t} = [\text{A}] k_d [\text{H}_2\text{O}]^n \left[(4 - 2K_{\text{eq}(\text{eff})} P_{\text{CO}_2(\text{eq})})(\theta - \theta_{\text{eq}}) - 4(\theta^2 - \theta_{\text{eq}}^2) \right] \quad (26)$$

$$= -[\text{A}] k_d [\text{H}_2\text{O}]^n (\theta - \theta_{\text{eq}}) \left[4(\theta + \theta_{\text{eq}} - 1) + 2K_{\text{eq}(\text{eff})} P_{\text{CO}_2(\text{eq})} \right] \quad (27)$$

Because $\theta + \theta_{\text{eq}} > 1$ is always satisfied in our area of interest, the sign of Eq.(27) confirms that CO_2 desorption occurs (i.e. $\frac{\partial \theta}{\partial t} < 0$) when $\theta > \theta_{\text{eq}}$ and CO_2 adsorption or adsorption occurs (i.e. $\frac{\partial \theta}{\partial t} > 0$) when $\theta < \theta_{\text{eq}}$. In terms of kinetics measurement experiments, $\theta - \theta_{\text{eq}}$ is a more convenient variable than θ . We can rewrite Eq.(26) into the following polynomial form (see section A.1 in the Supplementary Information):

$$\frac{\partial \theta}{\partial t} = [\text{A}] k_d [\text{H}_2\text{O}]^n \left[a_1(\theta - \theta_{\text{eq}}) + a_2(\theta - \theta_{\text{eq}})^2 \right] \quad (28)$$

where,

$$a_1 \equiv -\frac{(2\theta_{\text{eq}} - 1)(3 - 2\theta_{\text{eq}})}{1 - \theta_{\text{eq}}} \quad (29)$$

$$a_2 \equiv -4 \quad (30)$$

Eq.(28) indicates that surface sorption kinetics of moisture-controlled CO_2 sorbents is described as a linear combination of 1st and 2nd order kinetics. While a_2 is a constant value, a_1 is a function of the equilibrium loading state, θ_{eq} . Eq.(28) reduces to purely 2nd order kinetics only in case of $\theta_{\text{eq}} \sim 0.5$. The 1st or-

der kinetics is dominant when $|a_1/a_2| \gg 1$. In case that $\theta - \theta_{\text{eq}}$ is small, the linear term also dominates, even if $a_1 \sim a_2$. The isotherm equation Eq.(25) indicates that there is a characteristic pressure at the half loading state, i.e.,

$$\theta_{\text{eq}} \left(P_{\text{CO}_2(\text{eq})} = \frac{1}{2K_{\text{eq}(\text{eff})}} \right) = \frac{3}{4} \quad (31)$$

Thus,

$$|a_1/a_2| \begin{cases} < 3/4 & (\text{if } 1/2 < \theta_{\text{eq}} < 3/4) \\ = 3/4 & (\text{if } \theta_{\text{eq}} = 3/4) \\ > 3/4 & (\text{if } 3/4 < \theta_{\text{eq}} < 1) \end{cases} \quad (32)$$

Eq.(32) indicates that a_1 and a_2 are in the same order of magnitude at the half loading state.

2.2 Correction due to the change in the elementary reactions.

In this section, we derive the rate laws assuming that Eq.(1), Eq.(2) and Eq.(3) are elementary reactions. All of these are reversible reactions and we apply a pseudo steady-state approximation in which one reaction is regarded as a rate determining step and the other two are in quasi-equilibrium¹⁴. We refer to the case where Eq.(1), Eq.(2) or Eq.(3) is the rate-determining step as Case I, Case II and Case III, respectively. The rate law for each case can be derived as (see section A.2 in the Supplementary Information):

$$\frac{\partial \theta}{\partial t} = \begin{cases} \frac{[A]k_{-H}K_2[\text{H}_2\text{O}]^n}{K_1[\text{CO}_3^{2-}(\text{H}_2\text{O})_y]} \times \sum_{k=1}^2 a_k (\theta - \theta_{\text{eq}})^k & (\text{Case I}) \\ \frac{[A]k_{-1}[\text{H}_2\text{O}]^m}{[\text{HCO}_3^-(\text{H}_2\text{O})_x]} \times \sum_{k=1}^2 a_k (\theta - \theta_{\text{eq}})^k & (\text{Case II}) \\ \frac{[A]k_2[\text{H}_2\text{O}]^n}{K_H K_1 P_{\text{CO}_2}} \times \sum_{k=1}^2 a_k (\theta - \theta_{\text{eq}})^k & (\text{Case III}) \end{cases} \quad (33)$$

These rate laws indicate that an overall desorption rate constant k_d and an overall sorption rate constant k_a are no longer constant but functions of the concentrations or partial pressure of CO_2 (see section A.2 in the Supplementary Information), i.e.,

$$k_a = \begin{cases} \frac{k_H}{[\text{CO}_3^{2-}(\text{H}_2\text{O})_y]} & (\text{Case I}) \\ \frac{k_{-1}[\text{H}_2\text{O}]^{-n_2}}{[\text{HCO}_3^-(\text{H}_2\text{O})_x]} \left(\frac{K_{1(\text{AEM})}K_{H(\text{AEM})}}{K_{2(\text{AEM})}} \right) & (\text{Case II}) \\ \frac{k_{-2}}{P_{\text{CO}_2}} & (\text{Case III}) \end{cases} \quad (34)$$

and

$$k_d = \begin{cases} \frac{k_H}{[\text{CO}_3^{2-}(\text{H}_2\text{O})_y]} \left(\frac{K_{2(\text{AEM})}}{K_{1(\text{AEM})}K_{H(\text{AEM})}} \right) & (\text{Case I}) \\ \frac{k_{-1}[\text{H}_2\text{O}]^{-n_2}}{[\text{HCO}_3^-(\text{H}_2\text{O})_x]} & (\text{Case II}) \\ \frac{k_{-2}}{P_{\text{CO}_2}} \left(\frac{K_{2(\text{AEM})}}{K_{1(\text{AEM})}K_{H(\text{AEM})}} \right) & (\text{Case III}) \end{cases} \quad (35)$$

Note that in any case k_a/k_d takes the same value, i.e., $k_a/k_d = K_{H(\text{AEM})}K_{1(\text{AEM})}/K_{2(\text{AEM})}$. Here, we have the additional factor of either $1/[\text{CO}_3^{2-}(\text{H}_2\text{O})_y]$, $1/[\text{HCO}_3^-(\text{H}_2\text{O})_x]$ or $1/P_{\text{CO}_2}$ in the overall rate constants and the rate laws. A Taylor expansion of $\frac{1}{1-\theta}$ and $\frac{1}{2\theta-1}$ around $\theta \sim \theta_{\text{eq}}$ yields:

$$\frac{1}{[\text{HCO}_3^-(\text{H}_2\text{O})_x]} = \frac{1}{[A]} \frac{1}{2\theta-1} = \frac{1}{[A]} \sum_{k=0}^{\infty} \left(\frac{\theta - \theta_{\text{eq}}}{0.5 - \theta_{\text{eq}}} \right)^k \quad (36)$$

$$\frac{1}{[\text{CO}_3^{2-}(\text{H}_2\text{O})_y]} = \frac{1}{[A]} \frac{1}{1-\theta} = \frac{1}{[A]} \sum_{k=0}^{\infty} \left(\frac{\theta - \theta_{\text{eq}}}{1 - \theta_{\text{eq}}} \right)^k \quad (37)$$

Therefore, Eq.(36) and Eq.(37) gives a higher order correction to the rate law (Eq.(28)). Note that it is also possible that none of the three elementary reaction rate constants dominate and the pseudo quasi-equilibrium assumption cannot be applied. However, even in such a case, the kinetics equations should include both the 1st and 2nd order terms in order to satisfy the isotherm equation (Eq.(24)) at $\theta = \theta_{\text{eq}}$.

2.3 Correction due to a closed system.

If the system is open and the partial pressure of CO_2 can be regarded as approximately constant over the sorbent, P_{CO_2} in Eq.(21) is independent of θ . However, experiments for measuring kinetics are often performed in a closed system which changes the observed kinetics. In this system, the total volume is some finite value V_g . The volume of a sorbent is denoted by V_{AEM} . Assuming an ideal gas, P_{CO_2} can be expressed as a function of θ according to the mass conservation law for carbon in a closed system as

$$P_{\text{CO}_2} V_g = (n_{\text{tot}} - n_{\text{AEM}})RT \quad (38)$$

where, n_{tot} and n_{AEM} represent the amount of DIC in the whole system and that of DIC in a sorbent, respectively. R is the gas constant and T denotes temperature. Substituting $n_{\text{AEM}} = \theta[A]V_{\text{AEM}}$ into Eq.(38) yields

$$P_{\text{CO}_2} = P^* - P_{\text{AEM}}^* \theta \quad (39)$$

where,

$$P^* \equiv \frac{n_{\text{tot}}RT}{V_g} \quad (40)$$

and

$$P_{\text{AEM}}^* \equiv [A]RT \left(\frac{V_{\text{AEM}}}{V_{\text{g}}} \right) \quad (41)$$

P^* corresponds to partial pressure of CO_2 when all the DIC is transferred to the gaseous phase. Note that the open system is also included in this model as the limit of a very small P_{AEM}^* . Substituting Eq.(40) into Eq.(21) and some arrangement of terms (see section A.3 in the Supplementary Information) yields:

$$\frac{\partial \theta}{\partial t} = [A]k_d[\text{H}_2\text{O}]^n \left[a'_1(\theta - \theta_{\text{eq}}) + a'_2(\theta - \theta_{\text{eq}})^2 \right] \quad (42)$$

where,

$$a'_1 \equiv 2(2\theta_{\text{eq}} - 1)(K_{\text{eq}(\text{eff})}P_{\text{AEM}}^* - 2) - 2K_{\text{eq}(\text{eff})}P^* \quad (43)$$

$$a'_2 \equiv 2K_{\text{eq}(\text{eff})}P_{\text{AEM}}^* - 4 \quad (44)$$

In case that Eq.(1), Eq.(2) or Eq.(3) is the rate-determining step (Case I, Case II or Case III), the kinetics is described by Eq.(33) in which a_1 and a_2 are replaced with a'_1 and a'_2 , respectively. In the limit of $K_{\text{eq}(\text{eff})}P_{\text{AEM}}^* \ll 1$, a'_1 and a'_2 reduce to a_1 and a_2 .

3 Kinetic model part II: Chemical reaction - diffusion kinetics inside sorbents

Inside sorbents, chemical reaction and diffusion occur simultaneously. However, in certain limits, it is possible to eliminate chemical reactions in the interior of the sorbent from the transport equation. Specifically, this can be done if one is tracking the transport of DIC and can ignore the contributions of $[\text{OH}^-]$ and $[\text{CO}_2]$. In this case, the chemical reactions need only be considered on the boundary.

In this section, C_i , D_i , z_i and a_i represent concentration, diffusivity, electrochemical valence (negative for anions) and activity of each chemical species i , respectively. Activity coefficients γ_i are defined as $a_i = \gamma_i C_i$ ^{17,18}. In the absence of convective mass transfer, mass transfer is driven by a gradient in electrochemical potential, μ_i . The time-dependent behavior of each concentration in a sorbent can be described by the following Partial Differential Equations (PDEs)¹⁹:

$$\frac{\partial C_i}{\partial t} = \underbrace{-\vec{\nabla} \cdot \left(-\frac{D_i C_i}{RT} \vec{\nabla} \mu_i \right)}_{\text{mass transfer term}} + \underbrace{S_{i_1} + S_{i_2} + \dots + S_{i_N}}_{\text{chemical reaction kinetics term}} \quad (45)$$

Note that S_{i_m} summarizes the source term for the m -th reaction which i is subject to. Each reaction can refer to any and all other species involved. The explicit expressions of S terms in our specific case (moisture-controlled CO_2 sorption) are given in section B.1 in the Supplementary Information. μ_i in Eq.(45) is defined as¹⁹:

$$\mu_i(x,t) = \mu_i^0 + RT \ln a_i(x,t) + z_i F \phi(x,t) \quad (46)$$

where, F is the Faraday's constant, i.e., the absolute value of the charge on one mole of electrons. ϕ is an electrostatic potential, and μ_i^0 is a standard chemical potential. In simple cases, μ_i^0 is constant, and $a_i = C_i$ (in other words, $\gamma_i = 1$). This is the case for simple ideal gases or ideal solutions^{18,20}. However, in general the chemical potential can deviate substantially from such an ideal situation¹⁷. In this case, we choose to hold μ_i^0 constant, and absorb the deviation from ideality into the activity a_i . It should be noted, however, that in some cases it may be advantageous to account for the deviation from ideality by allowing μ_i^0 to be a function of spatial coordinates or concentrations and eliminate the distinction between a_i and C_i . In the following, μ_i^0 is a constant (thus, $\vec{\nabla} \mu_i^0 = \vec{0}$) and a_i is a variable that depends directly or indirectly on spatial and temporal coordinates. Substituting Eq.(46) into Eq.(45) yields¹⁸:

$$\frac{\partial C_i}{\partial t} = -\vec{\nabla} \cdot \left[-D_i \left(\vec{\nabla} C_i + C_i \vec{\nabla} (\ln \gamma_i) \right) + \left(-z_i (D_i C_i) \frac{F}{RT} \vec{\nabla} \phi \right) \right] + S_{i_1} + S_{i_2} + \dots + S_{i_N} \quad (47)$$

In case of $a_i = C_i$ (i.e., $\gamma_i = 1$), Eq.(47) simplifies to the Nernst-Planck equations^{19,21,22,23,24}:

$$\frac{\partial C_i}{\partial t} = \underbrace{-\vec{\nabla} \cdot \left(-D_i \vec{\nabla} C_i \right)}_{\text{diffusion term}} - \underbrace{\vec{\nabla} \cdot \left(-z_i (D_i C_i) \frac{F}{RT} \vec{\nabla} \phi \right)}_{\text{migration term}} + \underbrace{S_{i_1} + S_{i_2} + \dots + S_{i_N}}_{\text{chemical reaction kinetics term}} \quad (48)$$

$$= -\vec{\nabla} \cdot \left(\vec{J}_{i(\text{diff})} + \vec{J}_{i(\text{mig})} \right) + S_{i_1} + S_{i_2} + \dots + S_{i_N} \quad (49)$$

where,

$$\vec{J}_{i(\text{diff})} \equiv -D_i \vec{\nabla} C_i \quad (50)$$

$$\vec{J}_{i(\text{mig})} \equiv -z_i (D_i C_i) \frac{F}{RT} \vec{\nabla} \phi \quad (51)$$

$\vec{J}_{i(\text{diff})}$ and $\vec{J}_{i(\text{mig})}$ denote a molar diffusion flux and a molar migration flux of chemical species i , respectively. Their units are $[\text{mol m}^{-2} \text{s}^{-1}]$ in SI units. Note that the migration flux can be also expressed in terms of an electrochemical mobility u_i according to the Nernst-Einstein equation $u_i = \frac{D_i F}{RT}$ ^{21,18} as:

$$\vec{J}_{i(\text{mig})} = u_i z_i C_i \vec{E} \quad (52)$$

where, $\vec{E} (= -\vec{\nabla} \phi)$ denotes an electric field. Eq.(52) means that an electrochemical mobility u_i has a physical meaning as a proportionality factor that indicates how much flux is driven when an electric field \vec{E} is applied to chemical species i with the electrochemical valence of z_i and the concentration of C_i . It is also possible that one defines the mobility u_i as $\vec{J}_{i(\text{mig})} = u_i z_i C_i F \vec{E}$ and instead describe the Nernst-Einstein equation as $u_i = \frac{D_i}{RT}$ ²⁵. In any

cases, an corresponding electric current $\vec{T}_{i(\text{diff})}$ and $\vec{T}_{i(\text{mig})}$ can be calculated from a molar flux $\vec{J}_{i(\text{diff})}$ and $\vec{J}_{i(\text{mig})}$ as $\vec{T}_{i(\text{diff})} = Fz_i \vec{J}_{i(\text{diff})}$ and $\vec{T}_{i(\text{mig})} = Fz_i \vec{J}_{i(\text{mig})}$. Note that the Nernst-Einstein equation assumes ideal solutions²¹.

If the assumption of $a_i \sim C_i$ is not valid, the application of Eq.(48) can result in gross errors and violate second-law constraints. For example, it is possible to create a model of a perpetual motion machine that pumps a chemical species from one side of a membrane to the other against a chemical potential. For details see section B.4 in the Supplementary Information.

In this paper and the previous paper focused on equilibrium conditions¹³, the condition $a_i \sim C_i$ is satisfied, as long as the equilibrium constants do not change. In contrast to earlier efforts which varied equilibrium constants to capture moisture sensitivity of the sorbent^{26,27}, in this model, we treat the hydrated state of the various ions as a simple bound state and keep the equilibrium coefficients constant. This simple model of hydration is clearly an approximation that can only be justified by experimental observation. Implicit in the model is a stoichiometric relationship between hydration water and ions, and a mass balance between free water and hydration water. To the extent that this assumption is not valid, there will be correction to the model, which have to be discovered by experiment. The observation of the moisture-swing phenomenon assures that at least these corrections are not so large as to cancel out the moisture-swing phenomenon. However, it will require further work to obtain a better estimate of the size of these corrections. In this paper, we build an analytic model assuming $a_i \sim C_i$.

An alternative description of the phenomenon is to treat the water as a background field that modifies the energy states of the ions in proportion to the amount of water present. This will lead to a very similar model, but in this case the equation for the water flow would have to be separately considered. Furthermore, the equilibrium coefficients change with the concentration of the various species. As a result, one will have to account for spatial derivatives of μ_i^0 which cannot be treated as a constant any longer.

Based on Eq.(50) and Eq.(51), an electric current inside the membrane is expressed as¹⁹:

$$\begin{aligned} \vec{T} &= \sum_i \vec{T}_{i(\text{diff})} + \sum_i \vec{T}_{i(\text{mig})} = F \left(\sum_i z_i \vec{J}_{i(\text{diff})} + \sum_i z_i \vec{J}_{i(\text{mig})} \right) \quad (53) \\ &= - \left(\sum_i F z_i D_i \vec{\nabla} C_i + \sum_i z_i^2 (D_i C_i) \frac{F^2}{RT} \vec{\nabla} \phi \right) \quad (54) \end{aligned}$$

Local conservation of charge combined with the demand of charge neutrality assures that the net electric current is divergence free. If currents at the boundary are zero, all current flow lines in the interior must be closed, i.e., loops. Unless there are time-varying magnetic fields that drive these currents, the finite mobility of ions assures rapid decay of such loop currents. Be-

cause of such damping, in most cases the net charge current inside an AEM is zero. Therefore, $\vec{\nabla} \phi$ can be expressed as:

$$\vec{\nabla} \phi = - \frac{RT \sum_i z_i D_i \vec{\nabla} C_i}{F \sum_i z_i^2 D_i C_i} \quad (55)$$

By substituting Eq.(55) into Eq.(48), we obtain^{26,27}:

$$\begin{aligned} \frac{\partial C_i}{\partial t} &= \underbrace{-\vec{\nabla} \cdot (-D_i \vec{\nabla} C_i)}_{\text{diffusion term}} + \underbrace{S_{i_1} + S_{i_2} + \dots + S_{i_N}}_{\text{chemical reaction kinetics term}} \\ &\quad - \underbrace{\vec{\nabla} \cdot \left(z_i (C_i D_i) \frac{\sum_i z_i D_i \vec{\nabla} C_i}{\sum_i z_i^2 D_i C_i} \right)}_{\text{migration term}} \quad (56) \end{aligned}$$

Because of our interest in carbon transport and carbon sorption, we focus on the DIC rather than a concentration of each chemical species. In the limit that OH^- and CO_2 concentrations are negligible, this approach introduces a powerful constraint and there is no need to keep track of chemical reactions in the interior of the sorbent. For convenience, we define Dissolved Inorganic Carbon as Ions (DICI) as:

$$[\text{DICI}] \equiv [\text{HCO}_3^-] + [\text{CO}_3^{2-}] = [\text{DIC}] - [\text{CO}_2] \quad (57)$$

Combining the three PDEs (Eq.(56)) relevant to DIC (i.e., $[\text{CO}_2]$, $[\text{HCO}_3^-]$ and $[\text{CO}_3^{2-}]$) and taking advantage of the constraints from charge neutrality to recast $[\text{HCO}_3^-]$ and $[\text{CO}_3^{2-}]$ terms as $[\text{DICI}]$, $[\text{OH}^-]$ and $[\text{A}]$ terms, we obtain (for details see section B.1 in the Supplementary Information):

$$\frac{\partial [\text{DIC}]}{\partial t} = -\vec{\nabla} \cdot (\vec{J}_{\text{DIC}(\text{diff})} + \vec{J}_{\text{DIC}(\text{mig})}) \quad (58)$$

$\vec{J}_{\text{DIC}(\text{diff})}$ and $\vec{J}_{\text{DIC}(\text{mig})}$ represent a diffusion flux and a migration flux of DIC, which are explicitly calculated as:

$$\begin{aligned} \vec{J}_{\text{DIC}(\text{diff})} &= \vec{J}([\text{CO}_2]) + \vec{g}_1([\text{OH}^-]) \\ &\quad - (2D_{\text{HCO}_3^-} - D_{\text{CO}_3^{2-}}) \vec{\nabla} [\text{DICI}] \quad (59) \end{aligned}$$

$$\begin{aligned} \vec{J}_{\text{DIC}(\text{mig})} &= \left[D_{\text{HCO}_3^-} - 2D_{\text{CO}_3^{2-}} + g_2([\text{OH}^-]) - 2 \frac{[\text{DICI}]}{[\text{A}]} (D_{\text{HCO}_3^-} - D_{\text{CO}_3^{2-}}) \right] \\ &\quad \times \frac{2(D_{\text{CO}_3^{2-}} - D_{\text{HCO}_3^-}) \vec{\nabla} [\text{DICI}] + \vec{g}_3([\text{OH}^-])}{\frac{[\text{DICI}]}{[\text{A}]} (2D_{\text{HCO}_3^-} - 4D_{\text{CO}_3^{2-}}) - D_{\text{HCO}_3^-} + 4D_{\text{CO}_3^{2-}} + g_4([\text{OH}^-])} \quad (60) \end{aligned}$$

where,

$$\vec{f}([\text{CO}_2]) \equiv -D_{\text{CO}_2} \vec{\nabla}[\text{CO}_2] \quad (61)$$

$$\vec{g}_1([\text{OH}^-]) \equiv -(D_{\text{HCO}_3^-} - D_{\text{CO}_3^{2-}}) \vec{\nabla}[\text{OH}^-] \quad (62)$$

$$g_2([\text{OH}^-]) \equiv \frac{[\text{OH}^-]}{[A]} (2D_{\text{CO}_3^{2-}} - D_{\text{HCO}_3^-}) \quad (63)$$

$$\vec{g}_3([\text{OH}^-]) \equiv (2D_{\text{CO}_3^{2-}} - D_{\text{HCO}_3^-} - D_{\text{OH}^-}) \vec{\nabla}[\text{OH}^-] \quad (64)$$

$$g_4([\text{OH}^-]) \equiv \frac{[\text{OH}^-]}{[A]} (D_{\text{OH}^-} + D_{\text{HCO}_3^-} - 4D_{\text{CO}_3^{2-}}) \quad (65)$$

In Eq.(59) and Eq.(60), we neglected only $[\text{H}^+]$ terms but still include $[\text{CO}_2]$ and $[\text{OH}^-]$ terms. In many applications, contributions from carbon dioxide and hydroxide ions (i.e., \vec{f} , \vec{g}_1 , g_2 , \vec{g}_3 and g_4) can be regarded as negligible compared to DIC. In this approximation, $[\text{DIC}] \sim [\text{DIC}]$ and Eq.(58) substantially simplifies to the following single non-linear diffusion equation including only one variable, θ . After some rearrangement of terms (see section B.1 in the Supplementary Information), we obtain:

$$\frac{\partial \theta}{\partial t} \sim -\vec{\nabla} \cdot (-D_{\text{eff}} \vec{\nabla} \theta) \quad (66)$$

where,

$$D_{\text{eff}} \equiv \frac{D_{\text{HCO}_3^-} D_{\text{CO}_3^{2-}}}{D_{\text{HCO}_3^-} - 2D_{\text{CO}_3^{2-}}} \times \left(-1 + \frac{2(D_{\text{HCO}_3^-} - D_{\text{CO}_3^{2-}})}{2\theta(D_{\text{HCO}_3^-} - 2D_{\text{CO}_3^{2-}}) - (D_{\text{HCO}_3^-} - 4D_{\text{CO}_3^{2-}})} \right) \quad (67)$$

D_{eff} can be interpreted as a coupled interdiffusion coefficient^{21,28} or an effective diffusivity of total carbon inside a sorbent. The effective diffusivity D_{eff} is a function of not only $D_{\text{HCO}_3^-}$ and $D_{\text{CO}_3^{2-}}$ but also of θ itself. Only in case of $D_{\text{HCO}_3^-} = D_{\text{CO}_3^{2-}}$, D_{eff} does not depend on θ and $D_{\text{eff}} = D_{\text{HCO}_3^-} = D_{\text{CO}_3^{2-}}$. The effective diffusivity satisfies the following relations:

$$D_{\text{eff}}(\theta = 0.5) = D_{\text{HCO}_3^-} \quad (68)$$

$$D_{\text{eff}}(\theta = 1) = D_{\text{CO}_3^{2-}} \quad (69)$$

Note that Eq.(68) and Eq.(69) are non-trivial relations. These two equations imply that the effective diffusivity reduces to the diffusivity of the carbonate ions when all the counter ions are the bicarbonate ions while the diffusivity of the bicarbonate ion represents the effective diffusivity when all the counter ions are the carbonate ions. Also note that, in case of $D_{\text{HCO}_3^-} = 2D_{\text{CO}_3^{2-}}$, D_{eff} still has θ dependency, i.e., $D_{\text{eff}}(D_{\text{HCO}_3^-} = 2D_{\text{CO}_3^{2-}}) = (3 - 2\theta)D_{\text{CO}_3^{2-}} = (3/2 - \theta)D_{\text{HCO}_3^-}$. In any case, D_{eff} takes values between $D_{\text{HCO}_3^-}$ and $D_{\text{CO}_3^{2-}}$ so that both charge neutrality and the condition of null current (i.e. the charge transport in the diffusion current is

cancelled out by the migration current) are satisfied.

The solution of Eq.(66) depends critically on imposed boundary conditions. Two particular cases are of interest. One is a transient CO_2 flux responding to temporally varying, spatially homogeneous boundary conditions, the other is a dynamic steady state of a stationary CO_2 flux driven by spatially varying, but temporally constant boundary conditions.

3.1 Transient CO_2 flux.

When the surrounding humidity changes over time but is spatially constant along the boundary, DIC enters or leaves the boundary as gaseous CO_2 . If the external humidity settles to a new constant value, the CO_2 flux through the boundary gradually vanishes. This is a transient CO_2 flux, which is denoted as $J_{\text{trans}}(t)$. In the experimental section of this paper, we are observing such transient CO_2 fluxes in the geometry of a flat sheet. In this case, we can reduce the transport PDE to a one dimensional system. Our boundary conditions are step-functions in partial pressure of water vapor while keeping the partial pressure of CO_2 constant.

In a regime where D_{eff} can be regarded approximately constant, Eq.(66) simplifies to a linear diffusion equation. For a flat sheet of a sorbent, i.e., in a one dimensional system, the solution of this PDE is (see section B.2 in the Supplementary Information)^{29,30}:

$$\theta(x,t) = \theta_{\text{eq}} + \sum_{n=1}^{\infty} \frac{2(\theta_{\text{eq}} - \theta_{\text{ini}})}{n\pi} \{(-1)^n - 1\} \sin\left(\frac{n\pi}{L}x\right) e^{-D_{\text{eff}}\left(\frac{n\pi}{L}\right)^2 t} \quad (70)$$

where, L denotes the thickness of a membrane. We define the carbon loading over a whole membrane as:

$$\langle \theta \rangle(t) \equiv \frac{1}{L} \int_0^L \theta(x,t) dx \quad (71)$$

Substituting Eq.(70) into Eq.(71) yields:

$$\frac{\langle \theta \rangle - \theta_{\text{eq}}}{\theta_{\text{ini}} - \theta_{\text{eq}}} = 8 \times \left[\frac{1}{1^2 \cdot \pi^2} e^{-D_{\text{eff}}\left(\frac{1\pi}{L}\right)^2 t} + \frac{1}{3^2 \cdot \pi^2} e^{-D_{\text{eff}}\left(\frac{3\pi}{L}\right)^2 t} + \dots \right] \quad (72)$$

As we see in section 5, this form is particularly useful for experimental data analysis. This ratio is initially equal to one and approaches zero as the system equilibrates with an imposed steady and boundary condition. We define $T_{1/2}$ as the time when the system has moved a half way from the initial state to the equilibrium state, i.e., the ratio is equal to one half:

$$T_{1/2} \equiv \frac{1}{D_{\text{eff}}} \left(\frac{L}{\pi} \right)^2 \ln \left[\frac{16}{\pi^2} \right] \quad (73)$$

When $t \gtrsim T_{1/2}$, only the first terms dominates in Eq.(72), namely,

$$\ln \left[\frac{\langle \theta \rangle - \theta_{\text{eq}}}{\theta_{\text{ini}} - \theta_{\text{eq}}} \right] \sim -D_{\text{eff}} \left(\frac{\pi}{L} \right)^2 t - \ln \left[\frac{\pi^2}{8} \right] \quad (74)$$

or,

$$\frac{\partial}{\partial t} \ln(\langle \theta \rangle - \theta_{\text{eq}}) \sim -D_{\text{eff}} \left(\frac{\pi}{L} \right)^2 \quad (75)$$

This analytic form (Eq.(75)) indicates the 1st order kinetics.

3.2 Continuous CO₂ pumping flux.

A stationary CO₂ flux can be maintained by spatially varying but temporally constant boundary conditions. In the case of a membrane or a flat sheet, which is represented by a one dimensional PDE, this means the boundary conditions at the two sides are different. Since both water vapor concentration and CO₂ concentration in the gas phase affect boundary conditions, it is theoretically possible to maintain a DIC flux that is in the opposite direction to that expected from a CO₂ concentration difference between the two sides of the membrane. We refer to such a flux as a pumping flux. To satisfy thermodynamic constraints such pumping fluxes must be accompanied by an associated water flux that follows the water concentration difference. In effect, the water flux pumps CO₂ uphill^{26,27}. Pumping fluxes are of obvious interest in designs of CO₂ capture apparatus that would allow for continuous operation. It is analogous to electro dialysis-based electrochemical CO₂ capture that transfers carbonate/bicarbonate ions from one side of the membrane to the other with help of an electric rather than chemical potential³¹.

To illustrate this concept we solve the transport equations Eq.(66) with the following boundary conditions which involve the relative humidity (RH) and P_{CO_2} at the surfaces of a membrane:

$$\theta(x=0) = \theta_{\text{eq}} \left(P_{\text{CO}_2}(x=0); K_{\text{eq}}(\text{eff}) (\text{RH}(x=0)) \right) \equiv \theta_0 \quad (76)$$

$$\theta(x=L) = \theta_{\text{eq}} \left(P_{\text{CO}_2}(x=L); K_{\text{eq}}(\text{eff}) (\text{RH}(x=L)) \right) \equiv \theta_L \quad (77)$$

When $D_{\text{HCO}_3^-}$ and $D_{\text{CO}_3^{2-}}$ can be regarded as approximately constant during an experiment, the analytic solution of Eq.(66) in a dynamic steady state with these boundary conditions can be derived as (see section B.3 in the Supplementary Information):

$$\begin{aligned} & -(\theta - \theta_0) + \frac{D_{\text{HCO}_3^-} - D_{\text{CO}_3^{2-}}}{D_{\text{HCO}_3^-} - 2D_{\text{CO}_3^{2-}}} \\ & \times \ln \left[\frac{2\theta(D_{\text{HCO}_3^-} - 2D_{\text{CO}_3^{2-}}) - (D_{\text{HCO}_3^-} - 4D_{\text{CO}_3^{2-}})}{2\theta_0(D_{\text{HCO}_3^-} - 2D_{\text{CO}_3^{2-}}) - (D_{\text{HCO}_3^-} - 4D_{\text{CO}_3^{2-}})} \right] \\ & = \frac{x}{L} \left\{ -(\theta_L - \theta_0) + \frac{D_{\text{HCO}_3^-} - D_{\text{CO}_3^{2-}}}{D_{\text{HCO}_3^-} - 2D_{\text{CO}_3^{2-}}} \right. \\ & \left. \times \ln \left[\frac{2\theta_L(D_{\text{HCO}_3^-} - 2D_{\text{CO}_3^{2-}}) - (D_{\text{HCO}_3^-} - 4D_{\text{CO}_3^{2-}})}{2\theta_0(D_{\text{HCO}_3^-} - 2D_{\text{CO}_3^{2-}}) - (D_{\text{HCO}_3^-} - 4D_{\text{CO}_3^{2-}})} \right] \right\} \quad (78) \end{aligned}$$

Therefore, the amplitude of a CO₂ pumping flux can be expressed as:

$$\begin{aligned} & J_{\text{pump}}(D_{\text{HCO}_3^-}, D_{\text{CO}_3^{2-}}) \\ & = -\frac{D_{\text{HCO}_3^-} D_{\text{CO}_3^{2-}}}{L(D_{\text{HCO}_3^-} - 2D_{\text{CO}_3^{2-}})} [A] \left\{ -(\theta_L - \theta_0) + \frac{D_{\text{HCO}_3^-} - D_{\text{CO}_3^{2-}}}{D_{\text{HCO}_3^-} - 2D_{\text{CO}_3^{2-}}} \right. \\ & \left. \times \ln \left[\frac{2\theta_L(D_{\text{HCO}_3^-} - 2D_{\text{CO}_3^{2-}}) - (D_{\text{HCO}_3^-} - 4D_{\text{CO}_3^{2-}})}{2\theta_0(D_{\text{HCO}_3^-} - 2D_{\text{CO}_3^{2-}}) - (D_{\text{HCO}_3^-} - 4D_{\text{CO}_3^{2-}})} \right] \right\} \quad (79) \end{aligned}$$

In case of $D_{\text{HCO}_3^-} \sim D_{\text{CO}_3^{2-}} (\equiv D)$, Eq.(78) and Eq.(79) reduce to:

$$\frac{\theta - \theta_0}{\theta_L - \theta_0} \sim \frac{x}{L} \quad (80)$$

and

$$J_{\text{pump}}(D) \sim -D \left(\frac{\theta_L - \theta_0}{L} \right) [A] \quad (81)$$

This is a solution for a linear diffusion equation in a dynamic steady state.

4 Kinetic model part III: Integration of the two limiting cases

We have derived the governing equations for two limiting cases of moisture-controlled CO₂ sorption kinetics, i.e., Eq.(28) for surface chemical reaction kinetics and Eq.(66) for interior chemical reaction-diffusion transport kinetics. In general, the kinetics lies between these two extremes. The easiest way to distinguish between these two kinetics in an experiment is to observe the dependence of kinetics on the thickness of a membrane. While surface chemical reaction kinetics is independent of the thickness, interior chemical reaction-diffusion transport kinetics is enhanced as the membrane gets thinner. However, without varying thickness of the membrane, it is not possible to differentiate between two cases. Both limits indicate that 1st order kinetics is dominant around $\theta \sim \theta_{\text{eq}}$. In either case one can define a single parameter

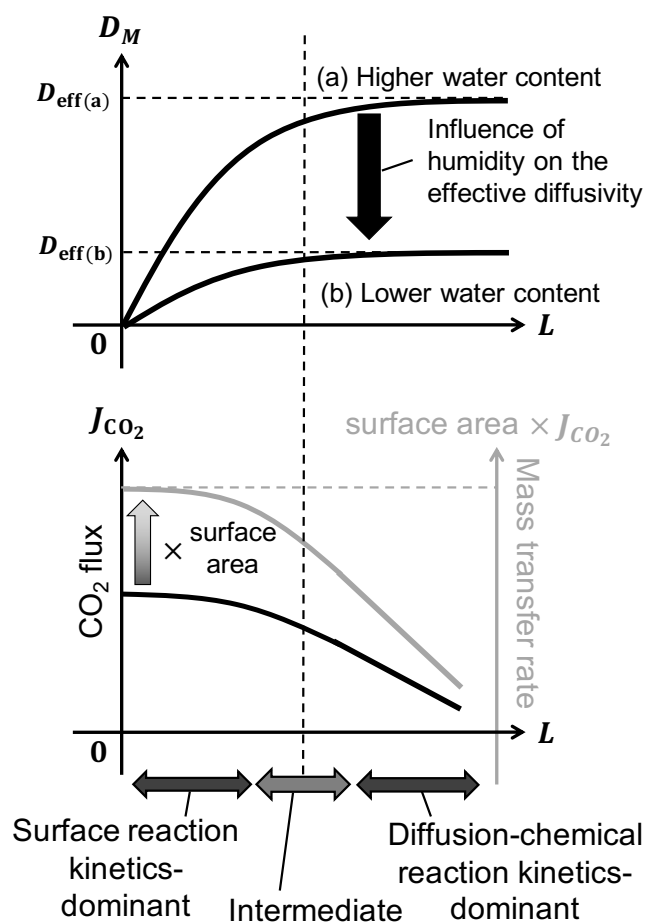


Fig. 1 A schematic diagram showing how the generalized effective diffusivity, CO₂ flux and mass transfer rate are influenced by the thickness of the AEM layer, L .

that characterizes the moisture-controlled CO₂ sorption kinetics. In this paper, we propose to define this single parameter that represents moisture-controlled CO₂ sorption kinetics as D_M by the following equation:

$$\frac{\partial}{\partial t} \ln \left[\frac{\langle \theta \rangle - \theta_{eq}}{\theta_{ini} - \theta_{eq}} \right] \equiv -D_M \left(\frac{\pi}{L} \right)^2 \quad (82)$$

D_M has the same dimension as diffusivities and converges to D_{eff} in the limit of a large thickness. By contrast, as the membrane gets thinner, the kinetics will be more dominated by surface chemical reaction kinetics, thus D_M starts deviating from D_{eff} and collapses to zero in the limit $L \rightarrow 0$. The optimal thickness of the membrane in practical applications can be given as a point where D_M starts deviating substantially from D_{eff} . D_M can be interpreted as a generalized effective diffusivity of carbon. Fig.(1) schematically shows how the generalized effective diffusivity is influenced by the thickness.

5 Experiments

In the previous sections, we have developed the analytic models describing the kinetics of CO₂ sorption and transport inside

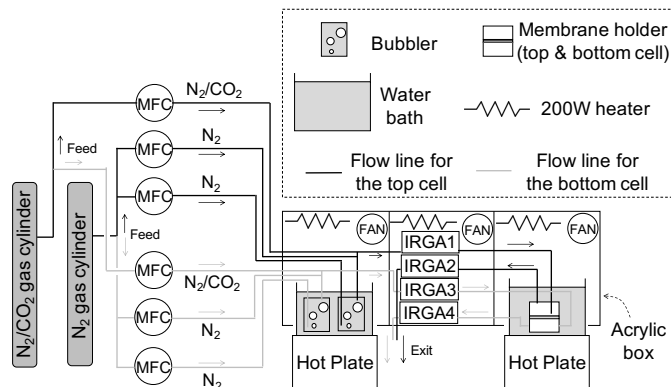


Fig. 2 The flow chart of the experimental apparatus. Mass flow controllers are used to control CO₂ and water vapor concentrations in the feed gas lines which provide two independent paths for gas to flow through a chamber divided by a sample membrane into two halves. A pair of Infrared Gas Analyzers are deployed in each line to measure concentration changes as the gases pass through the half cells.

moisture-controlled CO₂ sorbents. For flat membrane, we reduced the equations to a simple diffusion equation with a generalized diffusion coefficient, D_M , that incorporates the effects of chemical reaction kinetics and diffusive transport. We note that this generalized diffusion constant depends on the thickness of the membrane, L . Only in the limit where the chemical reaction is much faster than diffusive transport, the dependence of D_M on L vanishes. In this section, we report the results of kinetics measurement experiments for a moisture-controlled CO₂ sorbent and compare them to the analytic models.

For measuring kinetics of an anion exchange membrane, we can adopt experimental apparatus that is either based on a closed-system or an open-system¹⁰. As was discussed earlier, in a closed system, the measured kinetics can be affected by the volume of the system, which is not a material property but just an experimental condition that can vary from one experiment to another. Liu and Shen (2008) showed that even the Langmuir kinetics model can also have the 2nd order term in case of a closed system while it shows purely 1st order kinetics in an open system³². We have built open-system apparatus to measure the kinetics of moisture-controlled CO₂ without being influenced by experimental conditions.

5.1 Sample preparation and characterization

We use a commercial anion exchange membrane, Fumasep® FAA-3-50^{33 34 35 36 37} made by FuMA-Tech GmbH (Germany). This membrane is a non-brittle, thin flat sheet without any reinforcement. Applications include electrodialysis, desalination or alkaline fuel cells. The nominal thickness is 45-55 μm when it is dry³⁸. We measured the thickness at three points in an actual sample obtaining 47, 42, and 38 μm. Note that the membrane can swell when it is wet. In the experiment, we assume that the membrane thickness is 50 μm. This membrane is shipped from the manufacturer in a Br⁻ form for a long-term storage.

For preconditioning, we soak these membranes in 500 mL of

a 0.1 mol L⁻¹ K₂CO₃ solution or KHCO₃ solution for more than 12 hours to replace the counter ions with carbonate and/or bicarbonate ions. During this process, we observed the color of the membrane turned from brown to yellow.

After this procedure, we exposed membrane samples overnight to the ambient air in the laboratory to dry out and equilibrate with ambient levels of CO₂ and humidity. Given the low humidity in our laboratory in Arizona, we take this approximately as a dry state. Some samples were further processed by immersing them in DI water and equilibration with this wet environment. We then ion-exchanged the samples with sodium chloride solutions and determined the DIC and the IEC of a sample by titrating with hydrochloric acid. For the details see section C.1 and C.2 in the Supplementary Information. By comparing the DIC or θ of the wet and dry samples, we established the moisture-swing behavior of a membrane.

Table.(1) summarizes the measured θ and IEC of the dry and wet sample. The observed change of θ between a wet and a dry sample indicates that the preconditioned Fumasep® FAA-3-50 works as a moisture-swing material. The measured IEC per sample weight is 1.73±0.14 mmol/dryAEM-g for the dry sample and 1.35±0.11 mmol/dryAEM-g for the wet sample, both of which are comparable to the values in the manufacturer's technical data sheet³⁸, 1.6-2.0 mmol/dryAEM-g.

Table 1 Summary of the measured θ and IEC in the original samples by titration.

sample status	θ	IEC[mmol dry-g ⁻¹]
dry	1 ± 0.12	1.73 ± 0.14
wet	0.75 ± 0.08	1.35 ± 0.11

5.2 Main experimental system

5.2.1 Setup overview and instruments.

We designed and built a open-flow experiment. The flow chart is shown in Fig.(2). The custom membrane holder consists of a bottom cell and a top cell. The two cells are separated by the sample membrane that is held in place between two circular, flat rubber gaskets with an inner diameter of 7 cm, resulting in a nominal membrane area of 38.5 cm² (see Fig.(3)). There are two feed gas lines, one for the top cell and the other for the bottom cell. Each cell also has an exit line to the downstream gas analyzers and ultimately open air. The CO₂ and H₂O concentration in each feed gas can be controlled using a dry N₂ gas cylinder, a dry N₂(80%)-CO₂(20%) mixture gas cylinder, bubblers and six Mass Flow Controllers (MFC)³⁹ made by Alicat Scientific. The CO₂ and H₂O concentration in the two flow lines are measured before and after the membrane holder using four independent Infrared Gas Analyzers (IRGA)⁴⁰ made by LI-COR, which enables us to calculate the amount of CO₂ flux desorbed from or sorbed into the membrane sample. The membrane holder and the bubblers are placed in water baths where the temperature is controlled to 35.0 ± 0.2°C. The most of the length of the flow lines and the four IRGAs are contained in a acrylic box covered with thermal insulation to prevent condensation of water inside them. We refer to

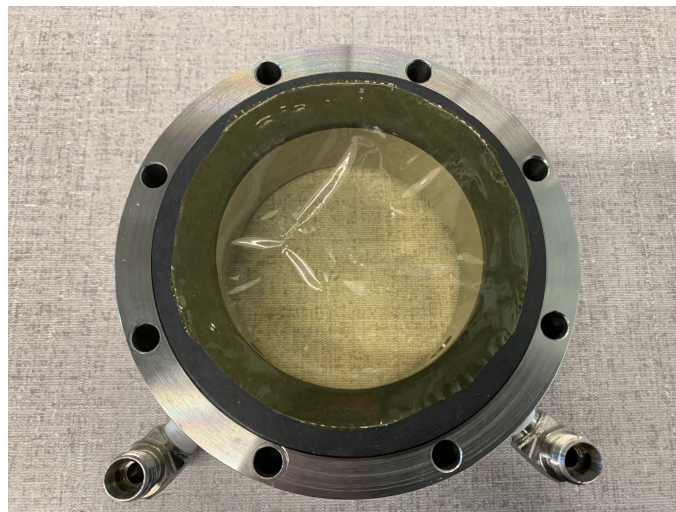


Fig. 3 A photograph of a yellowish Fumasep® FAA-3-50 membrane after preconditioning, being placed on a black custom rubber gasket (inner diameter = 7 cm and outer diameter = 10 cm) and the bottom half cell of the custom membrane holder. In an operation, the membrane is sandwiched between two such gaskets. The nominal area of the membrane is defined by the inner diameter of the gasket, i.e., 38.5 cm². The top and bottom half cells of the membrane holder are covered by acrylic plates of half-inch thickness during experiments. In the photograph, only the bottom half cell of the membrane holder is shown.

the four IRGAs as IRGA1, IRGA2, IRGA3 and IRGA4, according to Fig.(4). Since the gases are discharged into the environment outside of the acrylic box, the total pressure in each line is approximately that of the ambient environment throughout the system. See section C.3 in the Supplementary Information for more details about the experimental setup.

5.3 Experimental protocol

Once the sample is put in a membrane holder, we start heating the water baths that contain a membrane holder and bubblers to 35.0 °C and set mass flow rates of the input stream to achieve the desired flow rate and concentrations of CO₂ and water vapor. We wait for more than 10 hours until the exit concentrations match the input concentrations, the temperature in the whole system reaches its equilibrium, and the system is stable. After equilibrium is achieved, the humidity level in the feed gas is stepped up from dry to wet by adjusting mass flow rates of the dry and wet flow lines. We measure the transient CO₂ concentration and the water vapor concentration in the exist streams and calculate the desorption flux profile corresponding to this step-function humidity increase. Once the system reaches its new equilibrium with a stepped-up humidity, the input humidity is stepped down to the original level (i.e., dry environment) and the transient response is again observed. Throughout the experiments, the CO₂ concentrations in the two feed gas lines are kept at an equal and constant value, ~ 400 ppm (i.e. the ambient level in air), by setting the mass flow rates from a dry N₂(80%)-CO₂(20%) mixture gas cylinder to be 0.2 standard cm³ min⁻¹ out of the total mass flow rate 100.2 standard cm³ min⁻¹. Note that "standard cm³" stands for the volume measured under standard conditions, which in this

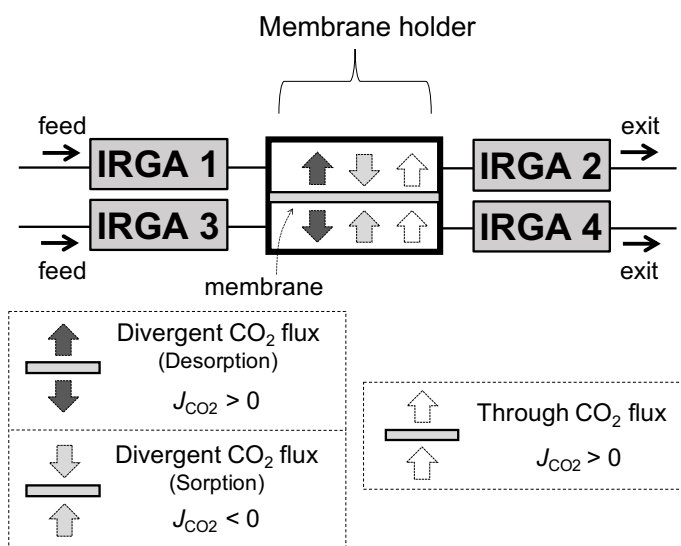


Fig. 4 The layout of the four IRGAs: IRGA1, IRGA2, IRGA3 and IRGA4, and diagrammatic description of various flow patterns.

context means 25°C and 1 atm³⁹.

5.4 Experimental conditions

We performed two experiments: Experiment (A) and Experiment (B) at different humidity levels measured at 35°C.

5.4.1 Experiment (A): Partial humidity swing.

In Experiment (A), the relative humidity level in the feed gas is stepped between 50% and 90%. This experiment avoids very dry conditions because of concerns over drastic reductions in diffusion coefficients under very dry conditions. In this regime, we expect the generalized effective diffusion coefficient to be approximately constant. This assumption will be justified below by the experimental results.

5.4.2 Experiment (B): Full humidity swing.

In Experiment (B), the relative humidity level in the feed gas is stepped between 5% and 90%. The driving force of the CO₂ flux is expected to be larger than in Experiment (A). However, the kinetics is shown strongly affected by a substantial reduction in ion diffusivities at low water content of a sorbent.

5.5 Data analysis protocol

5.5.1 Correction of IRGA readings to dry gas.

The humidity added from the bubblers slightly dilute the CO₂ concentration in the gas stream compared to the dry gas. To compensate for this dilution, we apply the following correction⁴¹:

$$\text{CO}_{2\text{cor}}[\text{ppm}] = \frac{\text{CO}_{2\text{raw}}[\text{ppm}]}{1 - \frac{\text{H}_2\text{O}_{\text{raw}}[\text{ppt}]}{1000}} \quad (83)$$

where, the subscript raw and cor represent the original reading from the IRGAs and the value after the correction, respectively.

Note that ppm for CO₂ and ppt for H₂O are the units of the IRGA reading, which represent parts per million and parts per thousand⁴⁰. They are molar fractions, not mass fractions. The calibration process based on Eq.(83) has been validated in control experiments using the same membrane holder but without a membrane sample (see Section C.4 in the Supplementary Information).

5.5.2 Mass transfer rates, through flows, divergent flows and associated fluxes

During the experiment, the total dry gas flow rate in each half cell (F_{top} or F_{bottom}) is held equal and constant at $F_{\text{top}} = F_{\text{bottom}} \equiv F = 100.2$ [standard cm³ min⁻¹]. For nitrogen or air, which are well approximated as an ideal gas, this flow rate is equivalent to $F = 70$ [μmol s⁻¹]. The corrected CO₂ concentration data are used to calculate the total CO₂ mass transfer rate between the membrane and the half cells:

$$\dot{m}_{\text{CO}_2, \alpha} = F_{\alpha} \times \Delta\text{CO}_{2\text{cor}, \alpha} \quad (\alpha = \text{top or bottom}) \quad (84)$$

where,

$$\Delta\text{CO}_{2\text{cor}, \alpha} = \begin{cases} \text{CO}_{2\text{cor}}(\text{IRGA2}) - \text{CO}_{2\text{cor}}(\text{IRGA1}) & (\alpha = \text{top}) \\ \text{CO}_{2\text{cor}}(\text{IRGA4}) - \text{CO}_{2\text{cor}}(\text{IRGA3}) & (\alpha = \text{bottom}) \end{cases} \quad (85)$$

From an experimental perspective, we are interested in the rate of the release or sorption of CO₂ on a membrane, $\dot{M}_{\text{CO}_2, \text{divergent}}$:

$$\dot{M}_{\text{CO}_2, \text{divergent}} = \dot{m}_{\text{CO}_2, \text{top}} + \dot{m}_{\text{CO}_2, \text{bottom}} \quad (86)$$

or the rate of the flow of CO₂ through the membrane, $\dot{M}_{\text{CO}_2, \text{through}}$:

$$\dot{M}_{\text{CO}_2, \text{through}} = (\dot{m}_{\text{CO}_2, \text{top}} - \dot{m}_{\text{CO}_2, \text{bottom}})/2 \quad (87)$$

In many experimental situations, it is useful to consider the flux into or through a sorbent material, for example, J_{CO_2} . This makes it easier to compare different geometries. To convert to a flux, one needs to divide mass transfer rate by the relevant area, S :

$$J_{\text{CO}_2, \beta} = \frac{\dot{M}_{\text{CO}_2, \beta}}{S_{\beta}} \quad (\beta = \text{divergent or through}) \quad (88)$$

where,

$$S_{\beta} = \begin{cases} 2A & (\beta = \text{divergent}) \\ A & (\beta = \text{through}) \end{cases} \quad (89)$$

A denotes the nominal membrane area. Note that we divided \dot{m}_{CO_2} by $2A$ for divergent fluxes, which accounts for the top and bottom surface of the membrane. In the case of a pure through-flux, $S = A$. However, the concept of a surface becomes less well-defined if membranes have internal structures. In general, the actual surface area of a sorbent material (S) could be much larger

than the nominal surface of the membrane (A). For example, if sorbent particles are embedded into membrane materials or sorbent membranes have very rough surfaces, then the ratio S/A can become very large. Similarly, for a through-flux, the actual areal size of a membrane (S) may be much smaller than the nominal cross section of the flow (A). If sorbent materials are embedded into the membrane matrix or contain pores, the effective area for the through-flux may be much smaller than the nominal area of a membrane, i.e., $S/A \ll 1$.

Based on our definitions, $J_{\text{CO}_2, \text{divergent}}$ is positive for desorption and negative for absorption. Our convention has CO_2 from the bottom to the top of the cell positive. The same sign convention applies for mass transfers and M_{CO_2} .

5.5.3 Data smoothing and drift compensations.

To suppress the noise level, a moving average filter with 375 seconds (i.e. about 6 minutes) is applied to $\Delta\text{CO}_{2, \text{cor}}$. $\Delta\text{CO}_{2, \text{cor}}$ is corrected by a small offset so that $\Delta\text{CO}_{2, \text{cor}} = 0$ at the initial equilibrium state. This correction compensates for a drift of IRGA readings over a long run and for the variance of the four IRGA readings. As for H_2O concentration data, only the moving average filter is applied.

5.5.4 Accumulative DIC and progress ratio.

By numerically integrating \dot{M}_{CO_2} from the initial time t_{ini} to the time t , the change in the DIC of the sample (ΔDIC) can be calculated as:

$$\Delta\text{DIC} = [A] \times \Delta\theta \times V_{\text{AEM}} \quad (90)$$

$$= - \int_{t_{\text{ini}}}^t \dot{M}_{\text{CO}_2, \text{divergent}} dt \quad (91)$$

The initial time t_{ini} is defined as the time right after a humidity step. To analyze the kinetics, we calculate $(\theta - \theta_{\text{eq}})/(\theta_{\text{ini}} - \theta_{\text{eq}})$ from $\Delta\text{CO}_{2, \text{cor}} (\equiv \sum_{\alpha} \Delta\text{CO}_{2, \text{cor}, \alpha})$. We refer to this ratio as a progress ratio because it is near one at early times and progresses towards zero as the system gets close to its equilibrium. This progress ratio is operationally well-defined even though θ , θ_{ini} and θ_{eq} are not known. Operationally, the ratio is defined as follows:

$$\frac{\theta - \theta_{\text{eq}}}{\theta_{\text{ini}} - \theta_{\text{eq}}} = \frac{\int_{t_{\text{ini}}}^{t_{\text{eq}}} \Delta\text{CO}_{2, \text{cor}} dt - \int_{t_{\text{ini}}}^t \Delta\text{CO}_{2, \text{cor}} dt}{\int_{t_{\text{ini}}}^{t_{\text{eq}}} \Delta\text{CO}_{2, \text{cor}} dt} \quad (92)$$

where, θ_{ini} and θ_{eq} represent the carbon loading status on the membrane at $t = t_{\text{ini}}$ and at $t = t_{\text{eq}}$, respectively. As time progresses, we expect θ to approach θ_{eq} . However, we will point to counter examples to such convergence in the discussion section. In any case one cannot wait for infinite time. Therefore we introduced a time cut-off t_{eq} when we assume $\theta \sim \theta_{\text{eq}}$.

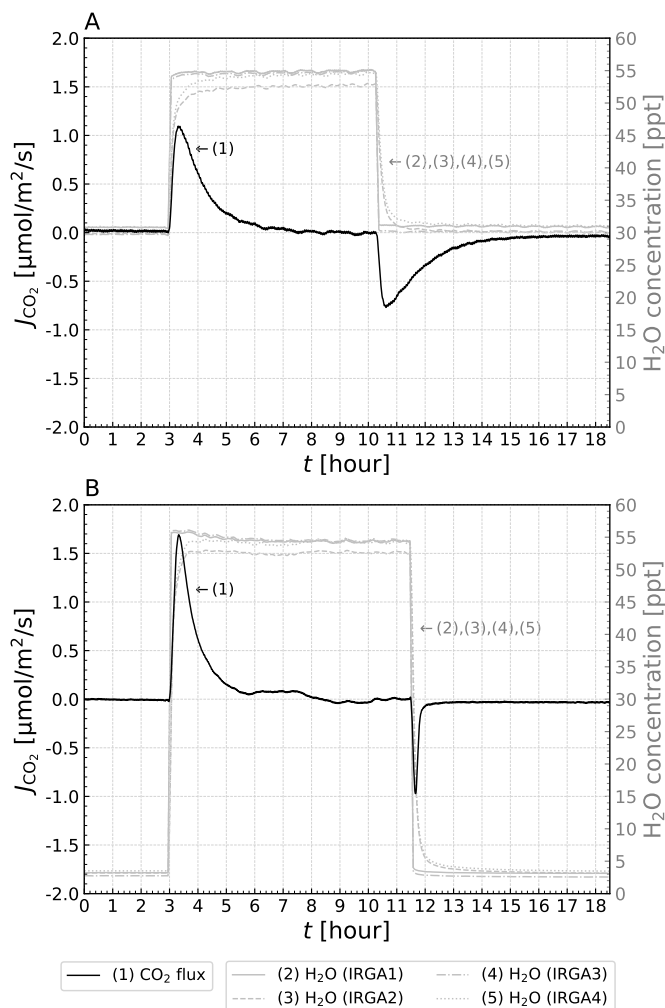


Fig. 5 H_2O profile in the feed gas and observed CO_2 flux profile in Experiment (A) and (B).

6 Results

6.1 Experiment (A)

Fig. (5) shows the input H_2O concentration profiles in the feed gas and the observed CO_2 flux responses in Experiment (A). The cumulative change of DIC in the membrane is displayed as a function of time in Fig.(6) for the sorption and desorption phase, respectively. The ΔDIC after stabilizing is 38.6 μmol for the desorption phase and 33.1 μmol for the absorption phase. Ideally, both values should be the same. One explanation of the difference could be that even after 6 hours the system has not yet reached equilibrium. Another possible explanation could be inaccuracies in measuring CO_2 concentrations. In general, the measurement accuracy for cumulative amounts is lower in an open-system experiment than in a closed-system experiment¹⁰. For example, integration of a 1 ppm offset over 5 hour in an open-flow experiment with the total dry gas flow rate in each half cell of $F = 70 \mu\text{mol s}^{-1}$ results in 2.5 μmol error in DIC. Nevertheless, we chose an open-flow system because of its advantages for the analysis of the kinetics.

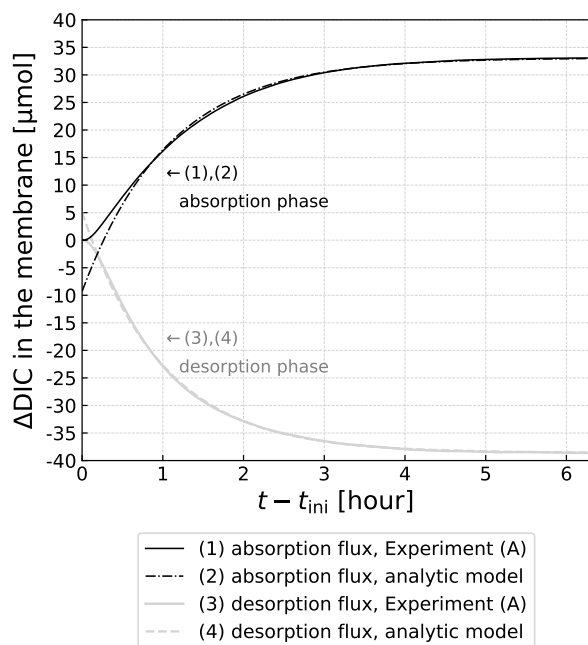


Fig. 6 Cumulative amount of DIC in the membrane calculated from the data of Experiment (A).

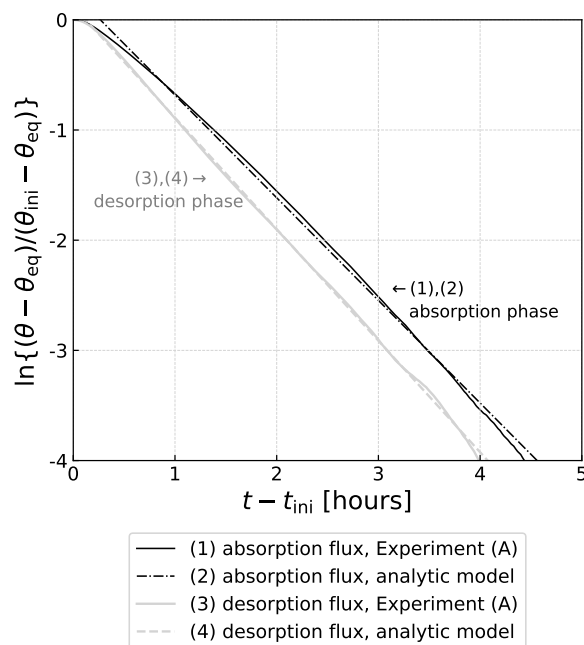


Fig. 7 Comparison between the measured progress ratio defined in the text for Experiment (A) and 1st order analytic models.

Fig. (7) shows the plot of $\ln[(\theta - \theta_{eq})/(\theta_{ini} - \theta_{eq})]$ against time. If the kinetics follows a 1st order model, the data should fall on a straight line. In Experiment (A), both the desorption and sorption flux are well fit by 1st order kinetics. The generalized effective diffusivity D_M defined in Eq.(82) is calculated from the slopes in Fig. (7). Table(2) summarizes the result and also provides the half-time $T_{1/2}$. D_M is slightly larger in desorption phase. This agrees with the expectation that ionic diffusivities are higher in anion exchange materials with higher water content^{42,43}.

6.2 Experiment (B)

Experiment (B) observed a very different behavior than Experiment (A) (see Fig. (7)). When the environment was changed from wet to very dry, a CO_2 sorption flux was still observed but it rapidly decayed to zero. As a result, the sorbed amount of CO_2 is only 12% of the desorbed CO_2 . This suggests the sorption was frustrated before equilibrium was reached.

Table 2 Summary of the calculated values of the generalized effective diffusivity of carbon in the membrane (D_M) and the half-time ($T_{1/2}$).

Humidity change	$D_M [\text{m}^2 \text{s}^{-1}]$	$T_{1/2} [\text{m}]$	$\Delta\text{DIC} [\mu\text{mol}]$	phase
30 → 55 ppt	7.1×10^{-14}	28.6	38.6	Desorption
55 → 30 ppt	6.6×10^{-14}	31.1	33.1	Absorption
3 → 55 ppt	N/A	N/A	43.9	Desorption
55 → 3 ppt	N/A	N/A	5.4	Absorption

7 Discussion

7.1 Characterization of moisture-controlled CO_2 sorption kinetics

In Experiment (A), we observed that both transient sorption and desorption CO_2 fluxes are well fit by 1st order kinetics. In this experiment, RH is always larger than 50% at 35 °C. Therefore, one can characterize the moisture-controlled CO_2 sorption kinetics of this system by a single parameter that combines contributions from both surface chemical reaction kinetics and interior diffusive transport kinetics. From a theoretical perspective, we have demonstrated that chemical reaction kinetics for moisture-controlled CO_2 sorption is a linear combination of 1st and 2nd order kinetics, plus higher order corrections that depend on which reaction is the rate-determining step. Pure 2nd order kinetics is expected only at $\theta_{eq} \sim 0.5$; otherwise, 1st order kinetics dominates as long as $\theta \sim \theta_{eq}$. The model of chemical reaction-diffusion kinetics also indicates the 1st order kinetics at around $\theta \sim \theta_{eq}$ as long as the effective diffusivity does not vary too much. Therefore, the theoretical models and the experimental observation are consistent.

From the experimental data, we calculated the generalized effective diffusivity D_M defined in Eq.(82). For a specific preconditioned commercial anion exchange membrane with thickness of 50 μm , D_M ranges from 6.6×10^{-14} to $7.1 \times 10^{-14} \text{ m}^2 \text{ s}^{-1}$. These values are very small compared to typical ionic diffusivity. For example, the diffusivity of NaCl in the anion exchange materials ranges from 5×10^{-11} to $2 \times 10^{-10} \text{ m}^2 \text{ s}^{-1}$ ^{20,44,45}. These low values of D_M explain why the moisture-controlled process is very slow.

There are three possibilities that could explain this substantially

smaller value: (1) a loss of water content decreases ion diffusivities significantly, (2) the chemical reaction kinetics significantly restrict the overall kinetics and (3) the assumption of $a_i \sim C_i$ is not very effective, which could allow for a counter flux that weakens the net carbon flux. Future investigation should identify the correct explanations. Understanding the cause of the slow kinetics is important because it directly affects practical applications of moisture-controlled CO₂ sorption.

One important next step would be to characterize the dependence of D_M on the thickness of a membrane. It would make it possible to differentiate between reaction rate limitations and diffusion rate limitations.

7.2 Practical humidity range for moisture-controlled CO₂ sorption

The sorption CO₂ flux profile data in a full humidity swing experiment (Experiment (B)) showed that exposure to very dry conditions significantly deteriorates the carbon transport kinetics. Although a full humidity swing was expected to sorb and desorb a larger amount of CO₂ than a partial humidity swing (Experiment (A)), the reverse turned out to be true, probably due to the choking of the ion transport. The very dry regime (RH~5%) does not only hamper mass transport but it also prevents the sorbent from reaching an equilibrium state. Experiment (A) revealed that a moderate to high humidity range (50% < RH < 90%) allows us to analyze the kinetics by using a simple 1st order model and a generalized effective diffusivity. Such a simple model facilitates predictions and allows for easy comparison of different sorbents. It also makes it easier to relate material characteristic to performance parameters and thus helps in engineering better sorbents.

Overall, the results of Experiment (A) and (B) suggest that practical humidity for moisture-controlled CO₂ sorption may have to stay away from extremely dry conditions. Further investigations have to identify the minimum humidity threshold that assures 1st order kinetics. The threshold depends on temperature and the material properties of a sorbent.

7.3 Impracticability of observing θ_{eq}

Measuring θ is complicated. Our experiments can easily measure the amount of CO₂ that enters or leaves the sorbent. However, these experiments cannot measure the initial loading of the sorbent nor determine the alkalinity or the ion exchange capacity of the sorbent. The advantage of the progress ratio $(\theta - \theta_{eq})/(\theta_{ini} - \theta_{eq})$ is that it only involves the differences that eliminates the offset and the ratio of these differences that eliminates the unknown scale factor associated with the alkalinity. However, the definition of this ratio assumes that after waiting for sufficiently long time, t_{eq} , θ approaches θ_{eq} . It is possible that this time is too long for practical purposes. Furthermore, if some kinetic parameters (e.g. rate constants or diffusivities) drop to almost zero at some point, the system can stagnate on the way to equilibrium and never reach it, i.e., $\theta(t = \infty) \neq \theta_{eq}$. We observed this phenomenon in a CO₂ sorption flux in Experiment (B). We speculate that, as water content inside a membrane drops significantly, the ion diffusivities decrease sufficiently to leave car-

bon stuck inside a membrane or locked out. This phenomenon is known more broadly. For example, Rogers et al. (1957) proposed to apply such behaviors to create a “permeability valve”⁴².

7.4 An estimated amplitude of a continuous CO₂ pumping flux

We have experimentally collected transient CO₂ flux data. Since the governing equations for a transient CO₂ flux and a continuous CO₂ pumping flux is the same, we can roughly estimate the amplitude of a continuous CO₂ pumping flux from transient CO₂ flux data. The transient CO₂ flux in response to a step function change in relative humidity over the sorbent is given as (for details and the definitions see section B.2 in the Supplementary Information):

$$J_{\text{pump}} \sim \left(\frac{4}{\pi^2}\right) \left(\frac{\Delta\theta_{\text{pump}}}{\Delta\theta_{\text{trans}}}\right) J_{\text{trans } T_{1/2}} \quad (93)$$

Namely, a continuous CO₂ pumping flux is about 2.5 times smaller than a transient flux at $t = T_{1/2}$. The result of Experiment (A) indicates $J_{\text{trans } T_{1/2}} \sim 0.7 \mu\text{mol m}^{-2}\text{s}^{-1}$. Substituting this value into Eq.(93) yields:

$$J_{\text{pump}} \sim 0.28 \left(\frac{\Delta\theta_{\text{pump}}}{\Delta\theta_{\text{trans}}}\right) [\mu\text{mol m}^{-2}\text{s}^{-1}] \quad (94)$$

It means that J_{pump} for this material at a certain condition can be predicted to be less than $< 0.1 \mu\text{mol m}^{-2}\text{s}^{-1}$ unless $\left(\frac{\Delta\theta_{\text{pump}}}{\Delta\theta_{\text{trans}}}\right) > 0.36$.

The analytic equation of J_{pump} (Eq.(79)) can be also used to estimate the amplitude of a continuous CO₂ pumping flux based on values of ion diffusivities. This equation indicates that the effective diffusivity has to be $\sim 10^{-12} \text{m}^2 \text{s}^{-1}$ to achieve J_{pump} of $6.3 \sim 10.0 \mu\text{mol m}^{-2}\text{s}^{-1}$ for a membrane with thickness of $50 \mu\text{m}$ (see section B.3 in the Supplementary Information). This value is more than 10 times larger than the observed D_M value for the specific membrane used in our experiments.

7.5 Complex sorbent geometries for air capture contactors

In our experiments, we focused on simple planar geometries of AEMs. These AEM membranes provide a convenient geometry for measuring material properties. Moreover, for direct air capture designs utilizing through-flux pumped by moisture gradients, a planar geometry of air-tight membrane is essential. However, there are many more geometries worth considering in the design of direct air capture contactors. For example, a sorbent can be made from sheets (2-dimensional, planar, $N = 2$), from fibers (1-dimensional, linear, $N = 1$) or from small particles or beads (0-dimensional, point-like, $N = 0$). The sorbent materials can be either densely packed or spaced far apart. L is the characteristic scale of the material, i.e., the thickness of a sheet or the diameter of a fiber or bead. In a contactor for direct air capture, a part of the volume is occupied by the sorbent; other parts are occupied by air or structural supports. While L characterizes the volume occupied by a single sheet, fiber or bead, d is the characteristic length scale of the volume that also includes the associated volume oc-

cupied by air or structural support. L^{3-N}/d^{3-N} is a measure of the volume fraction occupied by sorbents.

The geometry and the shape of the sorbent structure can be highly complex. The diffusion equations derived in this paper apply to the transport of DIC through the solid AEM sorbent in any geometry. The transport of carbon dioxide and water vapor through the air volume follows from fluid dynamic transport equations, which are not discussed here, but they help to determine the boundary conditions on the surface of the AEM. Quite often, transport of the air is so fast that one can assume nearly constant spatial boundary conditions on the surface of the sorbent. Even though transport may involve complex geometries, two critical parameters stand out: one is the total surface area, which sets the magnitude of the contact, and the other is the characteristic thickness of the sorbent, which sets the concentration gradient and thereby the flux through the surface. For a simple non-hierarchical geometries, there is a straight-forward relationship between the surface area density S , L and d :

$$S \propto \frac{L^{2-N}}{d^{3-N}} \quad (95)$$

Different application will find different optimizations, which also may be affected by the structural strength, integrity or durability of the AEM. Fig.(8) includes a brief summary of this discussion.

8 Conclusions

Many factors influence transport rates of DIC in AEMs. Fig.(8) summarizes the most significant impacts on transport rates. From a theoretical perspective, we have developed the analytic forms of the two extreme cases that govern the mass transport kinetics of moisture-controlled CO₂ sorption. The one is chemical reaction kinetics at the surfaces of a sorbent and the other is a combination of kinetics of chemical reactions and diffusion mass transport in the interior of the sorbent. In describing the time evolution of DIC, one can eliminate the interior chemical reaction terms as long as the contributions from CO₂ and hydroxide are small. A purely surface reaction model results in a linear combination of 1st order kinetics and 2nd order kinetics (Eq.(28)). The DIC in diffusion-dominated system can be described by a single non-linear diffusion equation (Eq.(66)) with an effective diffusivity D_{eff} (Eq.(67)) that combines the diffusion coefficient of bicarbonate and carbonate in a non-trivial manner. For example, as DIC approaches pure carbonate, the effective diffusivity becomes that of bicarbonate. In both cases, the 1st order term dominates as the loading status approaches equilibrium. Therefore, one can define a single parameter that characterizes the kinetics of moisture-controlled CO₂ sorption. In this paper, we also introduced a generalized effective diffusivity D_M that makes it possible to describe carbon transport in a flat membrane geometry even when the kinetics lies between the two extreme cases. D_M has the dimension of a diffusion coefficient, but it also incorporates the effect of reaction kinetics. As a consequence, D_M depends on the thickness of a membrane, L . It is defined by Eq.(82) and equivalent to D_{eff} when the thickness of a membrane is large. As the thickness gets

(I) Influence of sorbent property on transport rates	Dimension N			Thickness L
	$N = 2$	$N = 1$	$N = 0$	
Diffusion-bulk chemical reactions $J_{\text{CO}_2} \sim [A]D_{\text{eff}} \left(\frac{\pi}{L}\right)^2 (\theta - \theta_{\text{eq}})$	Sheet	Fiber	Bead	large
$J_{\text{CO}_2} \sim [A]D_M \left(\frac{\pi}{L}\right)^2 (\theta - \theta_{\text{eq}})$				
Surface chemical reactions $J_{\text{CO}_2} \propto \sum_{k=1}^2 a_k (\theta - \theta_{\text{eq}})^k$				
(II) Influence of sorbent geometry on transport rates				Spacing d
<ul style="list-style-type: none"> $\dot{M} = S \times J_{\text{CO}_2}$ is enhanced as S increases. Smaller L increases J_{CO_2} as long as L is not very small. 	Surface area density S depends on characteristic material size L and packing distance d .			$S \propto \frac{L^{2-N}}{d^{3-N}}$
(III) Influence of humidity on transport rates	Mass transport mode			
<ul style="list-style-type: none"> Divergent/through-flux <ul style="list-style-type: none"> At extremely dry conditions, $D_{\text{eff}} \rightarrow 0$. Rising humidity decreases the a_1/a_2 ratio. Through-flux <ul style="list-style-type: none"> The water gradient across a membrane decreases due to water flux across it. 	Divergent flux (desorption)	Divergent flux (sorption)	Through-flux (transport)	
	$J_{\text{CO}_2} > 0$	$J_{\text{CO}_2} < 0$	$J_{\text{CO}_2} > 0$	
(IV) Influence of experimental conditions on transport rates	Experimental condition			
<ul style="list-style-type: none"> In a closed-system, P_{CO_2} is a function of θ. For diffusive transports, the experimental conditions are implied by boundary conditions. 	<ul style="list-style-type: none"> Open-flow experiment 			Sample holder
	<ul style="list-style-type: none"> Closed-system experiment 			

Fig. 8 Schematic listing the four factors that have significant influences on transport rates, i.e., (I) sorbent property, (II) sorbent geometry, (III) humidity and (IV) experimental conditions. This figure also indicates how these four factors are related to other key parameters discussed in this paper such as sample thickness or mass transport modes.

smaller, D_M starts deviating from D_{eff} due to contribution from surface chemical reaction. D_M collapse to zero in the limit $L \rightarrow 0$. The thickness where D_M starts significantly deviates from D_{eff} can be interpreted as an optimal thickness of a membrane for practical applications of moisture-controlled CO₂ sorption.

The experiments have confirmed that the both transient sorption and desorption CO₂ flux profiles are fit well to a 1st order model as long as a very dry state (RH ~ 5%) was avoided. This observation agrees with the theoretical reasoning that the kinetics of moisture-controlled CO₂ kinetics can be represented by a single parameter. For the specific commercial anion exchange membrane with 50 μm thickness, the measured generalized effective diffusivity D_M ranges from 6.6×10^{-14} to 7.1×10^{-14} $\text{m}^2 \text{s}^{-1}$. These values are smaller than typical ionic diffusivities in anion exchange materials and can explain why moisture-controlled CO₂ sorption process is very slow. Such slow kinetics would be the largest issue to be addressed for practical applications of moisture-controlled CO₂ sorption. We proposed three possible causes for this slow behavior: (1) significant decrease of ion diffusivities due to low water content inside a sorbent, (2) the chem-

ical reaction kinetics is very slow and restricts the overall kinetics, or (3) the difference between a_i and C_i is not negligible. The next step would be to identify the main cause of such slow kinetics.

It has been also observed that carbon transport stops when humidity is decreased to a very low level (RH~ 5%). Therefore, practical operations of air capture systems should keep away from such very dry operating regimes. In such a very dry regime, the assumption of an approximately constant effective diffusivity is not valid and thus a 1st order model cannot be applied and resulting fit parameters would be unphysical. As long as one avoids such extremely dry conditions, the kinetics of moisture-controlled CO₂ sorption can be analyzed using a simple 1st order model and a generalized effective diffusivity. This will greatly simplify the characterization of the kinetics for moisture-controlled CO₂ sorbents and thus facilitate both designing novel sorbents and practical operations.

The measured transient CO₂ flux has been used to predict the amplitude of a continuous CO₂ pumping flux based on Eq.(66). The predicted value for the specific membrane is ~ 0.1 μmol m⁻² s⁻¹, which implies a very small flux for practical applications. One can also use the analytic equation of J_{pump} (Eq.(79)) to estimate the amplitude of the flux based on diffusivities of bicarbonate and carbonate ions. For example, this equation suggests that one needs the effective diffusivity to be ~ 10⁻¹² m² s⁻¹ to achieve J_{pump} of 6.3 ~ 10.0 μmol m⁻² s⁻¹ for a membrane with thickness of 50 μm. This value is more than 10 times larger than the observed D_M value for the specific membrane used in our experiments.

One approach to enhance a continuous CO₂ pumping flux is to make membrane thinner; however, a thinner membrane results in an increase of a water flux across the membrane, which makes it challenging to maintain a water gradient across the membrane to drive a continuous CO₂ pumping flux. Also, the restriction from the surface chemical reaction kinetics will start dominating for a very thin membrane, which we cannot enhance by making the membrane thinner. Therefore, it is important to raise the ion diffusivity relative to the water diffusivity and minimize limitations from reaction kinetics by speeding up reactions.

Author Contributions

Yuta Kaneko: Conceptualization, Investigation, Methodology, Visualization, Writing (original draft)

Klaus S. Lackner: Supervision, Validation, Writing (review & editing)

Conflicts of Interest

Klaus S. Lackner is a coinventor of IP owned by Arizona State University (ASU) that relates to certain implementations of direct air capture. Lackner also consults for companies that work on direct air capture. ASU has licensed part of its IP to Carbon Collect and owns a stake in the company. As an employee of the University, Lackner is a technical advisor to the company and in recognition also received shares from the company. Carbon Collect also supports DAC research at ASU.

Acknowledgements

This research has been performed as a part of the Mining Air for Fuels and Fine Chemicals (MAFF) project led by Arizona State University, together with Northern Arizona University and The University of Texas at Austin. The authors acknowledge insightful discussions with Dr. Justin Flory, Dr. Jennifer Lynn Wade, Dr. Matthew D. Green, Dr. Benny D. Freeman, Dr. Kristofer L. Gleason, Hoda Shokrollahzadeh Behbahani, Husain Mithaiwala, Horacio Lopez Marques and Winston Wang.

The authors also thank Dr. Kirk Thompson, Jason Kmon and Mani Modayil Korah for their support in designing and building the experimental apparatus and data acquisition systems.

The authors are also grateful for the support from the Center for Negative Carbon Emissions (CNCE) at Arizona State University.

The information, data, or work presented herein was funded in part by the Advanced Research Projects Agency-Energy (ARPA-E), U.S. Department of Energy, under Award Number DE-AR0001103. The views and opinions of authors expressed herein do not necessarily state or reflect those of the United States Government or any agency thereof.

Notes and references

- 1 K. Lackner, *The European physical journal. ST, Special topics*, 2009, **176**, 93–106.
- 2 K. S. Lackner and S. Brennan, *Climatic change*, 2009, **96**, 357–378.
- 3 E. S. Sanz-Pérez, C. R. Murdock, S. A. Didas and C. W. Jones, *Chemical reviews*, 2016, **116**, 11840–11876.
- 4 T. Wang, J. Liu, M. Fang and Z. Luo, *Energy Procedia*, 2013, **37**, 6096–6104.
- 5 J. Song, J. Liu, W. Zhao, Y. Chen, H. Xiao, X. Shi, Y. Liu and X. Chen, *Industrial & engineering chemistry research*, 2018, **57**, 4941–4948.
- 6 J. Song, L. Zhu, X. Shi, Y. Liu, H. Xiao and X. Chen, *Energy & fuels*, 2019, **33**, 6562–6567.
- 7 S. Douven, C. A. Paez and C. J. Gommers, *Journal of colloid and interface science*, 2015, **448**, 437–450.
- 8 T. Wang, J. Liu, H. Huang, M. Fang and Z. Luo, *Chemical engineering journal (Lausanne, Switzerland : 1996)*, 2016, **284**, 679–686.
- 9 T. Wang, J. Liu, K. S. Lackner, X. Shi, M. Fang and Z. Luo, *Greenhouse gases: science and technology*, 2016, **6**, 138–149.
- 10 D. P. Broom, O. Talu and M. J. Benham, *Industrial & engineering chemistry research*, 2020, **59**, 20478–20491.
- 11 T. Wang, K. S. Lackner and A. B. Wright, *Physical Chemistry Chemical Physics*, 2012, **15**, 504–514.
- 12 X. Shi, H. Xiao, K. Kanamori, A. Yonezu, K. S. Lackner and X. Chen, *Joule*, 2020, **4**, 1823–1837.
- 13 Y. Kaneko and K. S. Lackner, *Physical chemistry chemical physics : PCCP*, 2022, **24**, 14763–14771.
- 14 B. Peters, *Reaction rate theory and rare events*, Elsevier, Amsterdam, Netherlands, 2017 - 2017.

- 15 J. N. Butler, *Carbon dioxide equilibria and their applications*, Addison-Wesley, Reading, Mass, 1982.
- 16 T. Wang, K. S. Lackner and A. Wright, *Environmental science & technology*, 2011, **45**, 6670–6675.
- 17 E. A. Guggenheim, *Thermodynamics; an advanced treatment for chemists and physicists*, North-Holland Publishing Co., Amsterdam, 5th edn., 1967.
- 18 N. Lakshminarayanaiah, *Transport phenomena in membranes*, Academic Press, New York, 1969.
- 19 A. J. Bard, *Electrochemical methods : fundamentals and applications*, John Wiley, New York ;, 2nd edn., 2001.
- 20 J. Kamcev, D. R. Paul, G. S. Manning and B. D. Freeman, *Macromolecules*, 2018, **51**, 5519–5529.
- 21 F. G. Helfferich, *Ion exchange.*, McGraw-Hill, New York, 1962.
- 22 A. A. Moya and J. Horno, *The journal of physical chemistry. B*, 1999, **103**, 10791–10799.
- 23 V. Nikonenko, K. Lebedev, J. Manzanares and G. Pourcelly, *Electrochimica acta*, 2003, **48**, 3639–3650.
- 24 P. Sizat and G. Pourcelly, *Journal of membrane science*, 1997, **123**, 121–131.
- 25 J. S. Newman and N. P. Balsara, *Electrochemical systems / John S. Newman and Nitash P. Balsara.*, John Wiley & Sons Inc., Hoboken, NJ, Fourth edition. edn., 2021.
- 26 I. Rémy, *Numerical Simulation of a Carbon Dioxide Pump*, École Polytechnique Université Paris-Saclay technical report, 2014.
- 27 A. Robin, *Modelisation and Calibration of moisture sensitive beads in Carbon dioxide capture*, École Polytechnique Université Paris-Saclay technical report, 2015.
- 28 F. Helfferich and M. S. Plesset, *The Journal of chemical physics*, 1958, **28**, 418–424.
- 29 J. Crank, *The mathematics of diffusion.*, Clarendon Press, Oxford, 2nd edn., 1975.
- 30 R. Haberman, *Applied partial differential equations with Fourier series and boundary value problems*, Pearson, United States, Fifth edition. edn., 2019.
- 31 S. E. Renfrew, D. E. Starr and P. Strasser, *ACS catalysis*, 2020, **10**, 13058–13074.
- 32 Y. Liu and L. Shen, *Langmuir*, 2008, **24**, 11625–11630.
- 33 G. Chikvaidze, J. Gabrusenoks, J. Kleperis and G. Vaivars, *Journal of Physics: Conference Series*, 2007, **93**, 012026–.
- 34 P. V. Mazin, N. A. Kapustina and M. R. Tarasevich, *Russian journal of electrochemistry*, 2011, **47**, 275–281.
- 35 M. A. Vandiver, B. R. Caire, J. R. Carver, K. Waldrop, M. R. Hibbs, J. R. Varcoe, A. M. Herring and M. W. Liberatore, *Journal of the Electrochemical Society*, 2014, **161**, H677–H683.
- 36 C. Lo Vecchio, A. Carbone, S. Trocino, I. Gatto, A. Patti, V. Baglio and A. S. Aricò, *Polymers*, 2020, **12**, 2991–.
- 37 D. Henkensmeier, M. Najibah, C. Harms, J. Žitka, J. Hnát and K. Bouzek, *Journal of electrochemical energy conversion and storage*, 2021, **18**,.
- 38 FuMA-Tech GmbH, *Technical Data Sheet - fumasep FAA-3-50*, 2021.
- 39 Alicat Scientific, *MC/MCD-Series mass flow controller manual*.
- 40 LI-COR Biosciences, *LI-840A CO₂/H₂O Gas Analyzer Instruction Manual*.
- 41 LI-COR Biosciences, *The Importance of Water Vapor Measurements and Corrections*, LI-COR Biosciences Technical Report Application Note 129.
- 42 C. E. Rogers, V. Stannett and M. Szwarc, *Industrial and engineering chemistry*, 1957, **49**, 1933–1936.
- 43 J. Peng, A. L. Roy, S. G. Greenbaum and T. A. Zawodzinski, *Journal of power sources*, 2018, **380**, 64–75.
- 44 J. Kamcev, D. R. Paul, G. S. Manning and B. D. Freeman, *ACS applied materials & interfaces*, 2017, **9**, 4044–4056.
- 45 J. Kamcev, D. R. Paul, G. S. Manning and B. D. Freeman, *Journal of membrane science*, 2017, **537**, 396–406.